ISSN 0031-918X, Physics of Metals and Metallography, 2018, Vol. 119, No. 9, pp. 907–916. © Pleiades Publishing, Ltd., 2018.
Original Russian Text © R.A. Gaisin, V.M. Imayev, R.M. Imayev, 2018, published in Fizika Metallov i Metallovedenie, 2018, Vol. 119, No. 9, pp. 961–970.

## STRENGTH AND PLASTICITY

# Microstructure and Mechanical Properties of a Near-α-Titanium-Alloy/TiB Composite Prepared in situ by Casting and Subjected to Deformation and Heat Treatment

**R. A. Gaisin[a], *, V. M. Imayev[a], and R. M. Imayev[a]**

[a] *Institute for Metals Superplasticity Problems, Russian Academy of Sciences, Ufa, 450001 Russia*

**e-mail: ramilgaisin@gmail.com*

Received September 25, 2017; in final form, March 26, 2018

**Abstract**—This paper presents the results of our study of the microstructure and mechanical properties of a short-fiber composite material based on Ti/TiB prepared in situ by casting. We used a two-phase titanium alloy VT18U (Ti–6.8Al–4Zr–2.5Sn–1Nb–0.7Mo–0.15Si) as the matrix material for this study. The addition of boron and pure titanium into the titanium alloy led to the formation of 6.5 vol % TiB fibers. Two deformation treatments were used in this research. The first was isothermal forging in two directions (2D) at temperatures of the upper part of the α + β phase field to provide an elongation of TiB fibers along one direction; the second treatment was 3D forging at temperatures of the α + β phase field to ensure the refinement and random orientation of borides for fabricating material with isotropic properties as far as possible. The deformed semifinished samples of the composite materials and of the matrix alloy were annealed. The composite materials demonstrated noticeably higher strength and creep resistance compared to the matrix alloy and retained an acceptable plasticity. The microstructural studies of the fractured samples showed a high adhesion strength of boundaries between the matrix and the TiB fibers, which is retained even with increasing test temperature irrespective of the orientation and morphology of the borides. The failure of the composites begins with the breaking of borides and is followed by the ductile fracture of the matrix material.

*Keywords:* titanium alloys, short-fiber composites, microstructure, mechanical properties

**DOI:** 10.1134/S0031918X18090041

## INTRODUCTION

The creation of metal-matrix composite materials (CMs) reinforced with fibers and particles of various ceramic compounds is an efficient way to simultaneously increase the elastic modulus, strength, creep resistance, and wear resistance of titanium and its alloys [1–9]. The reinforcement components should possess high strength and high-temperature strength, chemical stability upon heating without the formation of intermediate phases, and thermal expansion coefficient close to that of titanium. As well as this, the boundary between the reinforcement component and the matrix should demonstrate high adhesion strength. Among various compounds used for reinforcement, titanium monoboride TiB is closest to indicated conditions (Table 1) [1–3]. The advantage of TiB is its formation in the fiber form upon the in situ preparation of the Ti/TiB composite using different methods. The fibers obtained have a semi-coherent boundary with the titanium matrix along their long axes; this boundary is characterized by a high adhesion strength, which prevents the separation of the fibers in the course of deformation of CMs [10, 11].

The Ti/TiB-based composite material is usually prepared using the compaction and sintering of powders of the titanium matrix and titanium diboride $TiB_2$, which forms titanium monoboride during chemical reaction with titanium. The CMs fabricated using this method are often characterized by insufficient plasticity and fracture toughness because of a residual porosity and increased impurities [3, 4]. An alternative simpler and cost-effective way to produce CMs based on Ti/TiB is a traditional casting, in which the TiB fibers are crystallized from the melt according to the eutectic reaction. However, when the boron content is higher than the eutectic one and the transition to hypereutectic composition takes place, the titanium monoboride is also formed in the form of coarse primary fibers, which impairs the main mechanical properties [12–17]. Therefore, for Ti/TiB-based CMs prepared by casting, there is a limitation on the content of boron and TiB volume fraction. Despite this, it has been shown for various CMs based on Ti/TiB (Ti/TiB + TiC, Ti/TiB + $La_2O_3$, etc.) that the presence of even a limited volume fraction of TiB fibers substantially increases the strength, elastic modulus,

**Table 1.** Properties of TiB in comparison with those of Ti and other reinforcement compounds of the titanium matrix [1–3]

| Characteristics | Ti | TiB | TiC | TiN | $TiB_2$ | SiC | $Si_3N_4$ | $B_4C$ | $Al_2O_3$ | $Ti_5Si_3$ |
|---|---|---|---|---|---|---|---|---|---|---|
| Density, g/cm$^3$ | 4.57 | 4.56 | 4.92 | 5.43 | 4.52 | 3.21 | 3.29 | 2.52 | 4.1 | 4.26 |
| Young's modulus, GPa | 110 | 550 | 460 | 390 | 529 | 420 | 320 | 449 | 350 | 156 |
| Ultimate tensile strength, GPa | 0.22 | 8 | 3.55 | – | – | 3.45 | <1 | – | – | – |
| Thermal expansion coefficient at 20°C ($\times 10^{-6}$), K$^{-1}$ | 8.8 | 8.6 | 7.4 | 9.35 | 6.4 | 4.3 | 3.2 | 4.5 | 8.1 | 7.3 |
| Intermediate phases forming at the boundary with Ti matrix | | – | – | – | TiB | $Ti_xSi$, TiC | $Ti_xSi$, TiN | TiB, TiC | $Ti_3Al$ | $Ti_xSi$ |

**Table 2.** Chemical composition of the investigated materials

| Material | Composition, in wt % | | | | | | | |
|---|---|---|---|---|---|---|---|---|
| | Ti | Al | Zr | Sn | Mo | Nb | Si | B |
| VT18U | Base | 6.8 | 4 | 2.5 | 0.7 | 1 | 0.15 | – |
| VT18U/TiB | Base | 6.8 | 4 | 2.5 | 0.7 | 1 | 0.15 | 1.2 |

creep resistance, and fatigue resistance at a certain decrease in the plasticity and fracture toughness [7–20].

According to the shear-lag model [21] developed for composites with uniformly distributed fibers strongly bound with the matrix, the strength increment depends on the orientation, shape (aspect ratio of the fibers), and volume fraction of the reinforcement material. The increase in its volume fraction, a high aspect ratio of the fibers, and their predominant orientation along the tensile axis are preferable to achieve maximum strengthening, elastic modulus, and creep resistance. At the same time, the different relative magnitude of the increment of strength properties at approximately the same volume fraction, texture, and morphology of borides for different titanium-based matrixes [14, 15, 22, 23] indicates that the shear-lag model is not universal when describing the mechanical behavior of the short-fiber CMs based on Ti/TiB. Another idea refers to the fabrication of isotropic Ti/TiB-based CMs, which can be more widely used compared to anisotropic CMs with preferably oriented TiB fibers.

This paper aims to investigate the Ti/TiB-based CMs and the development of methods of deformation and heat treatment to achieve elevated mechanical properties at temperatures of 500–600°C and higher. The high-temperature near-α titanium alloy VT18U having an operating temperature up to 600°C was taken as the matrix material. The amount of boron addition was 1.2 wt %, which corresponds to about 6.5 vol % of titanium monoboride. This paper is a continuation of an earlier work [23], in which the content of the added boron was optimized and the effects of strengthening and increasing the high-temperature strength in the case of CMs with preferably oriented TiB fibers were established quantitatively. In this work, we attempted to achieve an even sharper texture of fibers and to prepare an isotropic CM with refined borides with the subsequent study of mechanical properties and failure mechanisms. The resulting mechanical properties were compared with those of the matrix alloy.

## EXPERIMENTAL

The composition of the matrix alloy VT18U refined using the EDX method is given in Table 2. When preparing the VT18U/TiB CM, we added 1.2 wt % boron in the form of an amorphous powder (with a purity of ≥99.5%) and, additionally, titanium (with a purity of ≥99.74%) to compensate for its loss in the matrix because of the formation of titanium monoboride. 100-g composite ingots were prepared by argon-arc melting using a laboratory casting furnace. The temperature of the polymorphic transformation ($T_\beta$) of the materials was determined before the deformation and heat treatment by differential scanning calorimetry using a Netzsch STA 449F1 Jupiter calorimeter. In VT18U and VT18U/TiB, this temperature was $T_\beta \approx 1020$°C. Therefore the addition of boron has no noticeable effect on the temperature of the polymorphic transformation. We also observed this in the case of other titanium matrices [13, 15].

To achieve predominant orientation of TiB fibers, we used an isothermal forging in two directions (2D forging) at $T = 950$°C, so that the workpiece was elongated in the third direction during deformation. The deformation was performed using a hydraulic

**Table 3.** Heat treatment conditions of deformed workpieces

| Material | Heat treatment conditions* |
|---|---|
| VT8U | Annealing at $T = 980$°C ($\tau = 1$ h), $T = 550$°C ($\tau = 5$ h), $T = 650$°C ($\tau = 2$ h) |
| VT18U/TiB | Annealing at $T = 1050$°C ($\tau = 0.5$ h), $T = 550$°C ($\tau = 5$ h), $T = 650$°C ($\tau = 2$ h) |

* Air cooling after each annealing.

press equipped with an isothermal stamping block at a rate $\dot{\varepsilon} = 10^{-2}$–$10^{-3}$ s$^{-1}$ and a total strain $e \approx 4$.

To obtain randomly oriented fine borides, we used a three-dimensional (3D) isothermal forging at temperatures of 950 and 800°C. Stamps equiaxed in two directions were produced as a result. The deformation was carried out at a rate $\dot{\varepsilon} = 10^{-2}$–$10^{-3}$ s$^{-1}$ and a total strain $e \approx 4$. The cast workpieces of the VT18U alloy were deformed in the same way. The deformed workpieces were subjected to heat treatment (Table 3). The VT18U alloy was annealed in the $(\alpha + \beta)$ phase field to avoid the rapid growth of grains. The VT18U/TiB composite was first annealed in the $\beta$-phase field, then in the $\alpha + \beta$ field. The rapid growth of grains in the $\beta$ field in the case of the composite was prevented by the presence of fibers of titanium monoboride [15, 24].

We carried out the microstructural studies using a Mira-3 Tescan scanning electron microscope (SEM) in secondary electron (SE) or backscatter electron (BSE) mode. Using electron microscopic images, we estimated the volume fraction of TiB fibers, sizes of the initial $\beta$ grains and $\alpha/\beta$ colonies, and the thickness of plates. We analyzed the microtexture of the CMs after 2D forging using the electron backscatter diffraction (EBSD) method. The energy dispersive X-ray (EDS) analysis was carried out using an energy dispersive spectrometer (an attachment to SEM). Before studying the microstructure, we subjected the surface of the samples to mechanical and electrolytic polishing and insignificant etching. To estimate the aspect ratio $L/D$ of the borides, we subjected the surface of the CM samples after 2D and 3D forging to deep etching. The measurements were carried out by an ImageJ software using electron microscopic images.

The mechanical tensile tests of the VT18U and VT18U/TiB samples were carried out at $T = 20$–700°C. We used flat samples with a size of the gage part of $10 \times 3.5 \times 1.5$ mm, which were cut from materials after deformation and heat treatment using an electric-spark method. The samples were subjected to mechanical grinding and polishing before tests. We used at least three samples for each point.

We performed creep tests at $T = 550$–650°C, using two samples for each point. We tested flat samples having the gage part of $17 \times 3 \times 3$ mm for 50 h. The tests were carried out in air.

## RESULTS AND DISCUSSION

### *Initial Materials*

Figure 1 shows the microstructure of the VT18U alloy and VT18U/TiB composite in the initial cast state. The alloy in this state has a typical coarse-grained plate-like $(\alpha + \beta)$ structure with the size of the

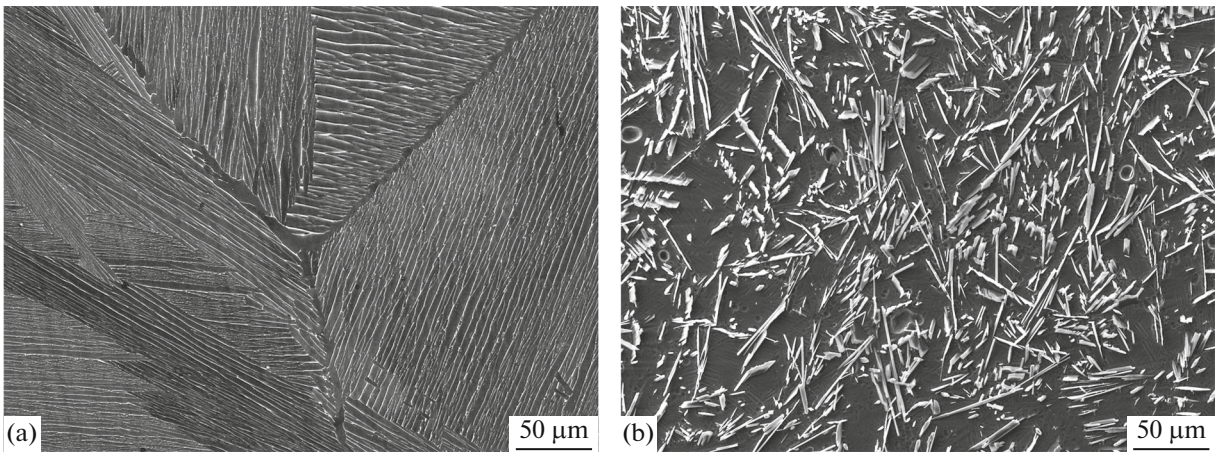


**Fig. 1.** Microstructure of the initial cast materials: (a) VT18U (SEM, BSE); (b) VT18U/TiB (SEM, EBSD), the surface after deep etching [23].

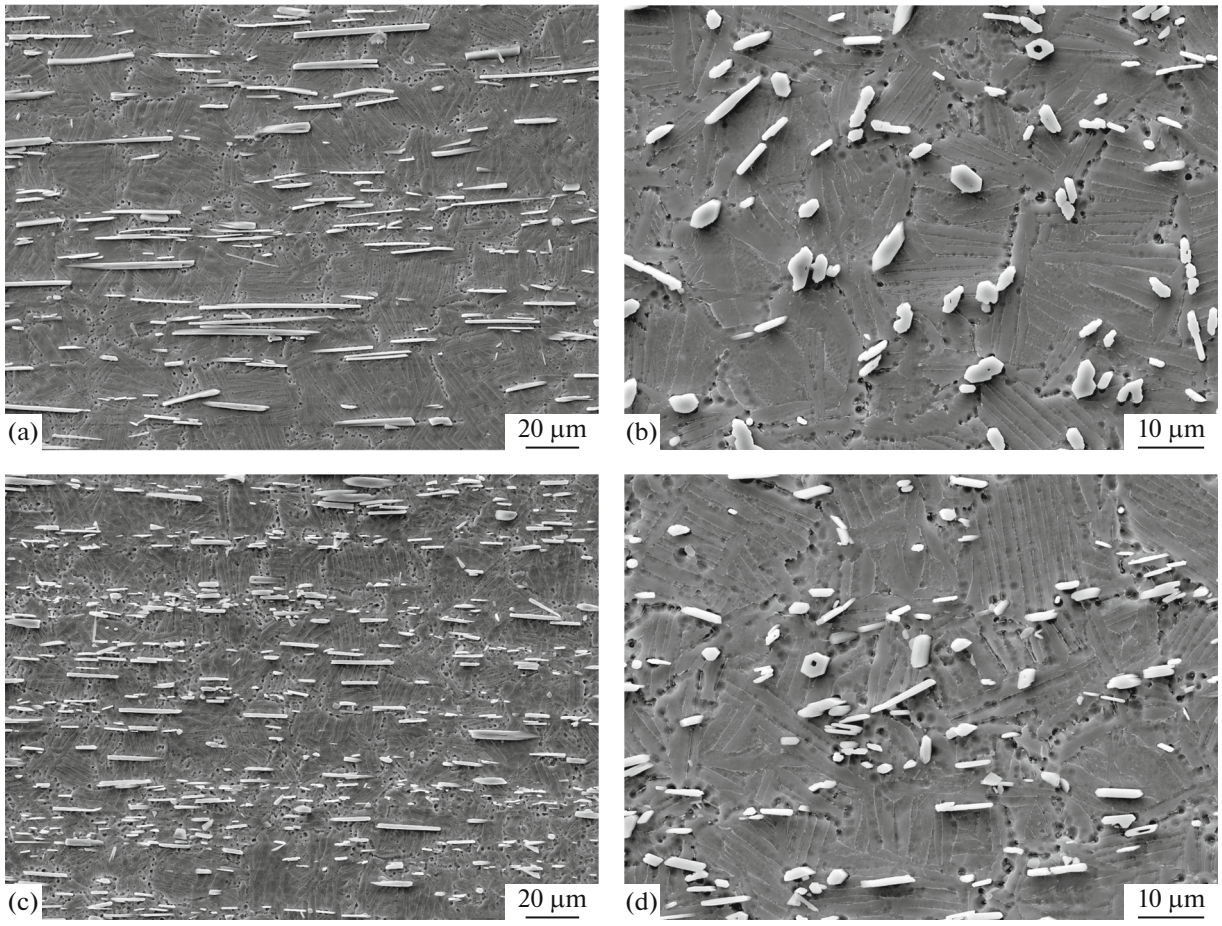


**Fig. 2.** Microstructure of VT18U/TiB after forging and heat treatment (SEM, EBSD): (a, b) after 2D forging and heat treatment; (c, d) after 3D forging and heat treatment: (a, c) longitudinal and (b, d) transverse sections of the deformed workpieces.

initial β grains $D_\beta$ ~ 1000 μm. The boron addition resulted in the formation of homogeneously distributed and randomly oriented short TiB fibers, the presence of which (as will be seen below) favors the refinement of the matrix structure. The size of borides is $L \times D$ = (10–200) × (0.5–5) μm; their volume fraction is 6.5%. The average aspect ratio of borides is $L/D \approx 30$ [23].

### *State of Materials after Deformation and Heat Treatment*

The VT18U alloy after deformation and heat treatment is characterized by a duplex structure consisting of primary α grains and β-transformed structure with an average size of grains/plate-colonies $d \approx 10$ μm. The composite after the 2D forging has a completely β-transformed plate-like structure with a size of α/β colonies $d$ = 10–50 μm and preferably oriented TiB fibers. The 3D forging also resulted in a completely β-transformed structure but with smaller α/β colonies ($d$ = 5–25 μm) and randomly oriented TiB fibers (Fig. 2).

The heat treatment with rapid heating into the β field, when the TiB fibers prevented the rapid growth of β grains, made it possible to obtain a relatively small size of α/β colonies. It was smaller in the case of the uniform 3D forging. We also noted that the borides were refined strongly as a result of the 3D forging and were much fewer in number than upon 2D forging. The intensive refinement of borides upon 3D forging is caused by the deformation scheme and by the decreased deformation temperature. The average aspect ratio of borides is $L/D \approx 6$ after 3D forging and $L/D \approx 17$ after 2D forging. Therefore the deformation led to a substantial refinement of borides upon 3D forging and less intensive refinement upon 2D forging. However, even after 3D forging, the aspect ratio of borides was higher than the critical value [25].

Figure 3 shows the TiB {010} and α-Ti $\{11\bar{2}0\}$ direct pole figures for the VT18U/TiB composite after 2D forging and heat treatment. The measurements showed that the [010] direction of TiB fibers after 2D forging was parallel to the drawing direction of the deformed workpiece; the maximum relative intensity

reaches 60.7 (Fig. 3a). In our earlier work [23], the relative intensity in the VT18U/TiB composite after 2D forging with a lower degree of strain ($e \approx 3$) reached 40.1. The [010] direction in TiB is known as the direction of the predominant growth of fibers because of the highest rate of boron diffusion along this axis [26]. This texture indicates that the long axes of TiB fibers are mainly oriented along the direction of drawing of the workpiece upon 2D forging. The measurements also revealed a rather sharp texture in the α phase after 2D forging (Fig. 3b): the $\langle 1\bar{1}20\rangle$ direction of α-Ti was parallel to the drawing direction of the workpiece; the relative intensity was 5.1. Note that the texture in the α phase at lower degree of strain ($e \approx 3$) was more diffuse [23].

We already know that the TiB fibers are oriented relative to the α phase of the titanium matrix as follows [7]: $[11\bar{2}0]_{Ti} \parallel [010]_{TiB}$, $(0001)_{Ti} \parallel (001)_{TiB}$, and $(1\bar{1}00)_{Ti} \parallel (100)_{TiB}$. The texture, therefore, correlates with the orientation relationship between the reinforcement agent and the matrix. It should be noted that this deformation treatment in the VT8/TiB composite led to the formation of a similar sharp texture of both fibers and the α phase [15], whereas we observed a less sharp texture in the VT25U/TiB-based composite [22]. We can conclude that after 2D forging the preferred orientation of TiB fibers is achieved and a high aspect ratio is retained; 3D forging results in the formation of randomly oriented and strongly refined borides. In both cases, the matrix material represented a completely β-transformed plate-like structure.

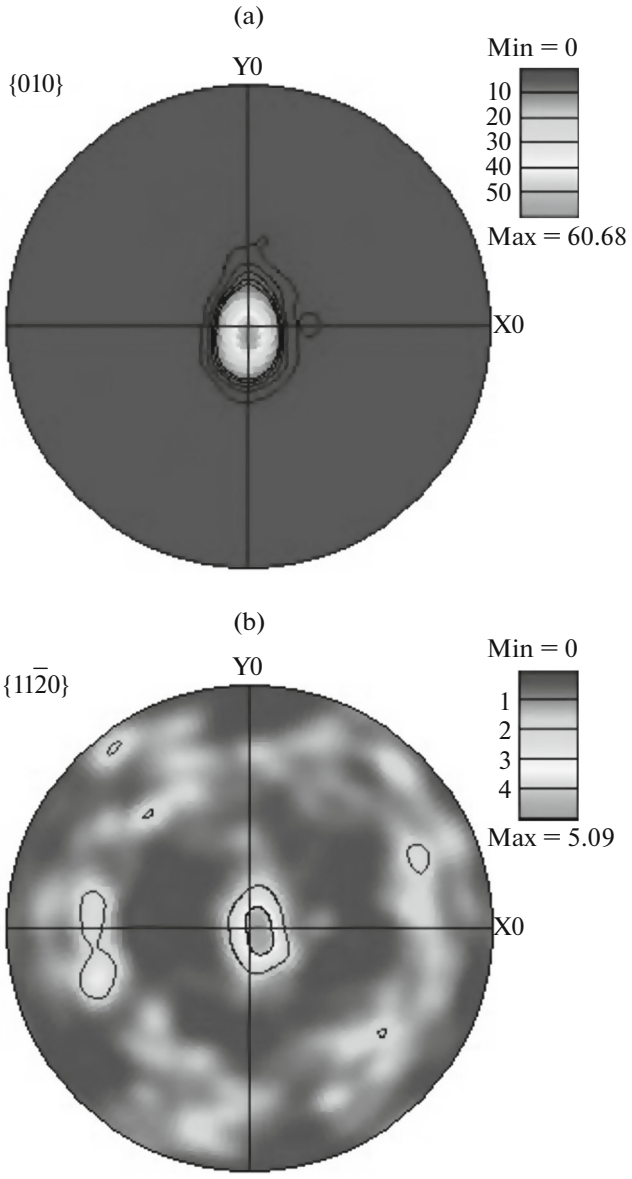


**Fig. 3.** Direct pole figures (a) {010} TiB and (b) $\{11\bar{2}0\}$ α-Ti obtained for the VT18U/TiB composite after 2D forging and heat treatment.

### *Mechanical Tensile Properties*

Figure 4 shows the mechanical tensile properties of the VT18U alloy and VT18U/TiB composite after deformation and heat treatment. The presence of 6.5 vol % TiB fibers and particles led to a significant increase in the strength characteristics. If we assume that the yield stress of the CM matrix and VT18U alloy (after deformation and heat treatment) is approximately the same, an increment in the yield stress at $T = 20$–$700$°C is 17.3–26.4% in the case of the randomly oriented TiB fibers and 23.3–32.0% in the case of the preferably oriented TiB fibers (Table 4). After the 2D forging with a lower degree of deformation, which led to a less sharp texture of TiB fibers, the yield-stress increment decreased slightly [23] (Table 4). A reduction of the texture sharpness of TiB fibers (with a decrease in the degree of deformation in the case of 2D forging and upon the transition to 3D forging) generally leads only to an insignificant decrease in the effect of strengthening caused by the presence of TiB fibers. The plasticity of the CM at room temperature ($\delta$ = 5.2–7.0%) only slightly depends on the orientation and degree of refinement of borides (Fig. 4). With an increase in the test temperature, the CM with refined borides (after 3D forging) has a greater plasticity at $T = 500$°C than that with preferably oriented borides. At $T = 600$–$700$°C, the difference in plasticity almost disappears.

Therefore, the presence of 6.5 vol % TiB fibers provides a substantial yield-stress increment, the relative value of which is retained up to $T = 700$°C. The plasticity of the CM is no less than $\delta = 5\%$ at room temperature. The retention of the contribution of the TiB fibers to the strengthening effect with an increase in the test temperature indicates the retention of the high

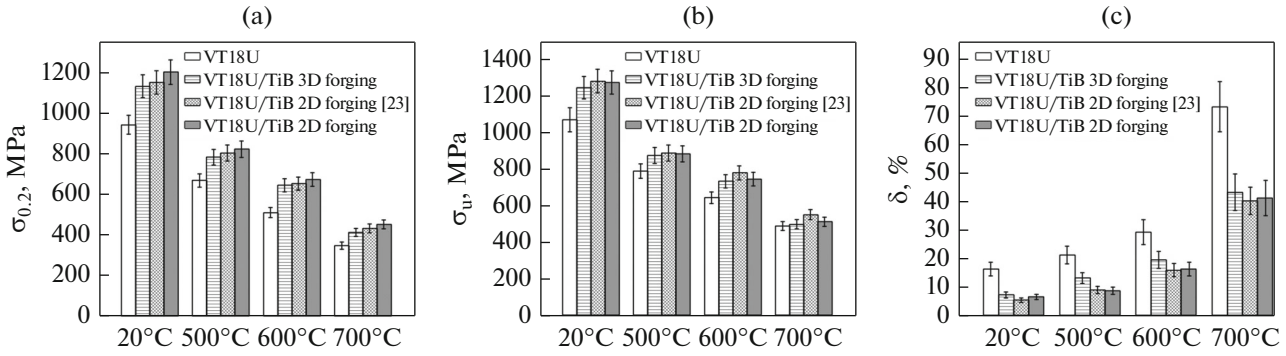


**Fig. 4.** Temperature dependences obtained for the VT18U alloy and VT18U/TiB composite after deformation and heat treatment: (a) yield stress $\sigma_{0.2}$; (b) ultimate tensile strength $\sigma_u$; and (c) relative elongation $\delta$.

adhesion strength of boundaries between the titanium matrix and TiB fibers at elevated temperatures [7, 22]. Another important conclusion is that the presence of the preferably oriented TiB fibers only insignificantly increases the strength compared to the CMs with randomly oriented refined borides even in the case of the sharp texture of fibers (strictly speaking, the values of the strength properties of the CMs in all three states are within the error limits).

In accordance with a shear-lag model for short-fiber CMs [15, 19–21], which presupposes a uniform distribution of fibers and high adhesion strength of the matrix/fiber boundaries, the yield-stress increment in CMs is proportional to the volume fraction of fibers and to their aspect ratio and to the orientation of fibers relative to the tensile axis:

$$\Delta\sigma_{0.2} = \sigma^{m}_{0.2} \times 0.5 \times V \times L/D \times C, \quad (1)$$

where $\Delta\sigma_{0.2}$ is the yield-stress increment in CM, $\sigma^{m}_{0.2}$ is the ultimate tensile strength of the matrix alloy, $V$ is the volume fraction of fibers, $L/D$ is the aspect ratio of fibers, and $C$ is the orientation factor, which can vary from 0 to 1.

The fact that the close values of the yield-stress increment in the CMs are observed after both 2D and 3D forging (followed by the same heat treatment) providing different aspect ratios $L/D$ and texture of fibers (see Table 4) suggests that the yield stress of the CM also depends on the average distance between borides. The intensive breaking (desintegration) of borides during 3D forging led to a decrease in the $L/D$ value by 3 times in comparison with the material subjected to 2D forging (Table 4). We can assume that this led to a decrease in the distance between borides, which likely compensated for the reduction of the strengthening because of the breaking of borides and their random orientation.

### *Creep Tests*

Creep tests performed at $T$ = 550–600°C showed that the CM demonstrates appreciably higher creep resistance than the matrix alloy (Fig. 5).

**Table 4.** Yield-stress increment obtained for the VT18U/TiB composite at various test temperatures in comparison with the matrix VT18U alloy ($\Delta\sigma_{0.2}$ is the yield-stress increment; $\sigma^{m}_{0.2}$ is the yield stress of the matrix material; and h/t is the heat treatment)

| State of the CM | Aspect ratio ($L/D$) | Relative intensity of texture of fibers (EBSD data) | $\Delta\sigma_{0.2}/\sigma^{m}_{0.2} \times 100$, % | | | |
|---|---|---|---|---|---|---|
| | | | 20°C | 500°C | 600°C | 700°C |
| 3D forging and h/t | 6 | – | 20.2 | 17.3 | 26.4 | 18.8 |
| 2D forging ($e \approx 4$) and h/t | 17 | 60.7 | 27.7 | 23.3 | 32.0 | 30.4 |
| 2D forging ($e \approx 3$) and h/t [23] | 20 | 40.1 | 22.3 | 20.3 | 28.0 | 24.6 |

We can see that the presence of borides has a positive effect in the case of preferable orientation of TiB fibers parallel to the loading axis and in the case of randomly oriented and refined borides. It is possible that the presence of refined borides uniformly distributed over the entire bulk of the material favors a more uniform distribution of stresses under conditions of creep than in the case of preferably oriented TiB fibers with a high aspect ratio $L/D$. In the last case, the stresses under the conditions of creep seem to be more localized and the positive effect of preferably oriented TiB fibers on the creep resistance decreases accordingly.

### *Fracture Behavior*

Figure 6 shows the microstructure of a composite subjected to 3D forging and heat treatment near and far from the fracture zone after tests at different temperatures. An extensive breaking of the TiB fibers occurred near the fracture zone at all test temperatures. A similar picture of fracture was observed earlier in composites based on Ti–6Al–4V, VT8, VT25U, and VT18U alloys [6, 15, 22, 23] with preferably oriented relatively long borides. Upon deformation, the short fibers in the VT18U/TiB CM after 3D forging are divided and refined into even shorter particles, which indicates the efficiency of the loading transfer from the matrix to stronger fibers. Far from the fracture zone, the breaking of borides occurred less intensely, which indicates a substantial localization of deformation at the final stage of deformation. Near the places of breaking of the TiB fibers, discontinuities were formed locally and in some cases the fibers were separated from the matrix. However, this did not lead to the rapid fracture of the entire CM, because the transfer of a part of the load from the matrix to fibers is retained, which follows from the multiple breaking of the fibers into a number of short particles. With an increase in the deformation temperature to 700°C and an attainment of high elongations ($\delta$ = 43%) (see Fig. 6), the character of breaking of the fibers remains unchanged in principle. The substantial strengthening effect caused by the presence of borides (Table 4) and their extensive breaking during deformation indicates the retention of a high adhesion strength of the boundaries between the TiB fibers and titanium matrix.

Figure 7 presents the fracture surface of tensile samples of the VT18U/TiB CM subjected to 3D forging followed by heat treatment. We noted that the fracture was predominantly ductile and there was no noticeable difference between the character of fracture at room temperature and at $T$ = 600°C after 2D and 3D forging [23]. We also noted that the unfavorably oriented borides promoted a brittle fracture by cleavage. However, in the case of the 3D forging (when the amount of such borides is greater), this did not lead to an increase in the brittle component in the fracture. It seems that the breaking of borides upon 3D forging decreased the negative effect of the unfavorably oriented borides on the fracture. On the whole, the mechanism of failure of the VT18U/TiB CM during tensile deformation at room and elevated temperatures was brittle fracture of TiB fibers followed by the ductile fracture of the matrix material. This is consistent with earlier works [8, 11, 15, 23].

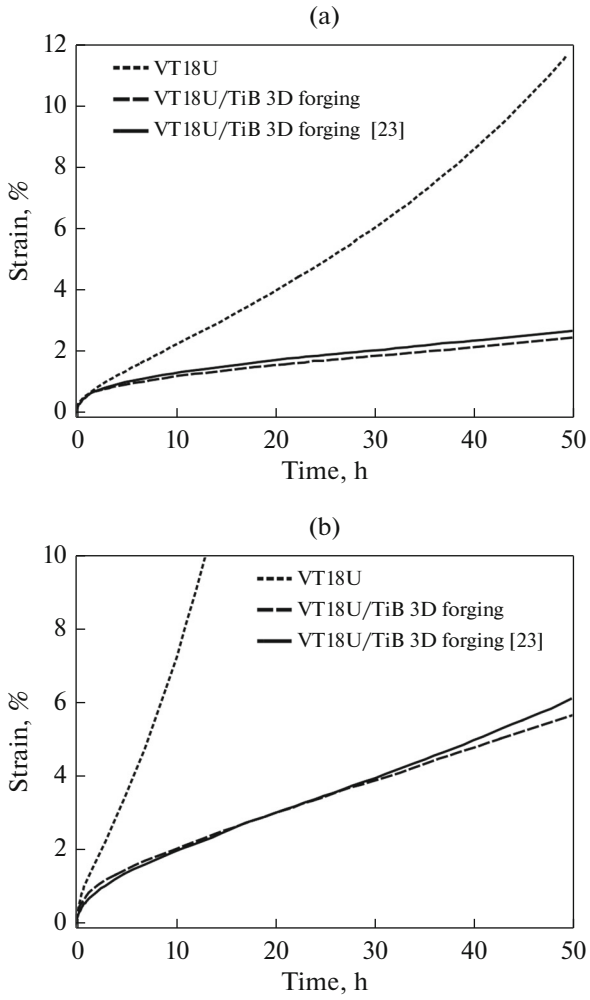


**Fig. 5.** Creep curves obtained for the VT18U alloy and VT18U/TiB composite: (a) $T$ = 550°C and $P$ = 400 MPa; (b) $T$ = 600°C and $P$ = 300 MPa.

Thus, in the case of the VT18U/6.5 vol % TiB CM, in addition to the possibility of preparation of a textured CM with preferably oriented TiB fibers characterized by a high aspect ratio, it is worth considering the idea of fabricating an isotropic CM with borides randomly oriented and refined during 3D forging. The mechanical properties of the VT18U/6.5 vol % TiB CMs with randomly oriented refined borides are not inferior to those of the CMs with preferably oriented borides. This is likely explained by the more uniform

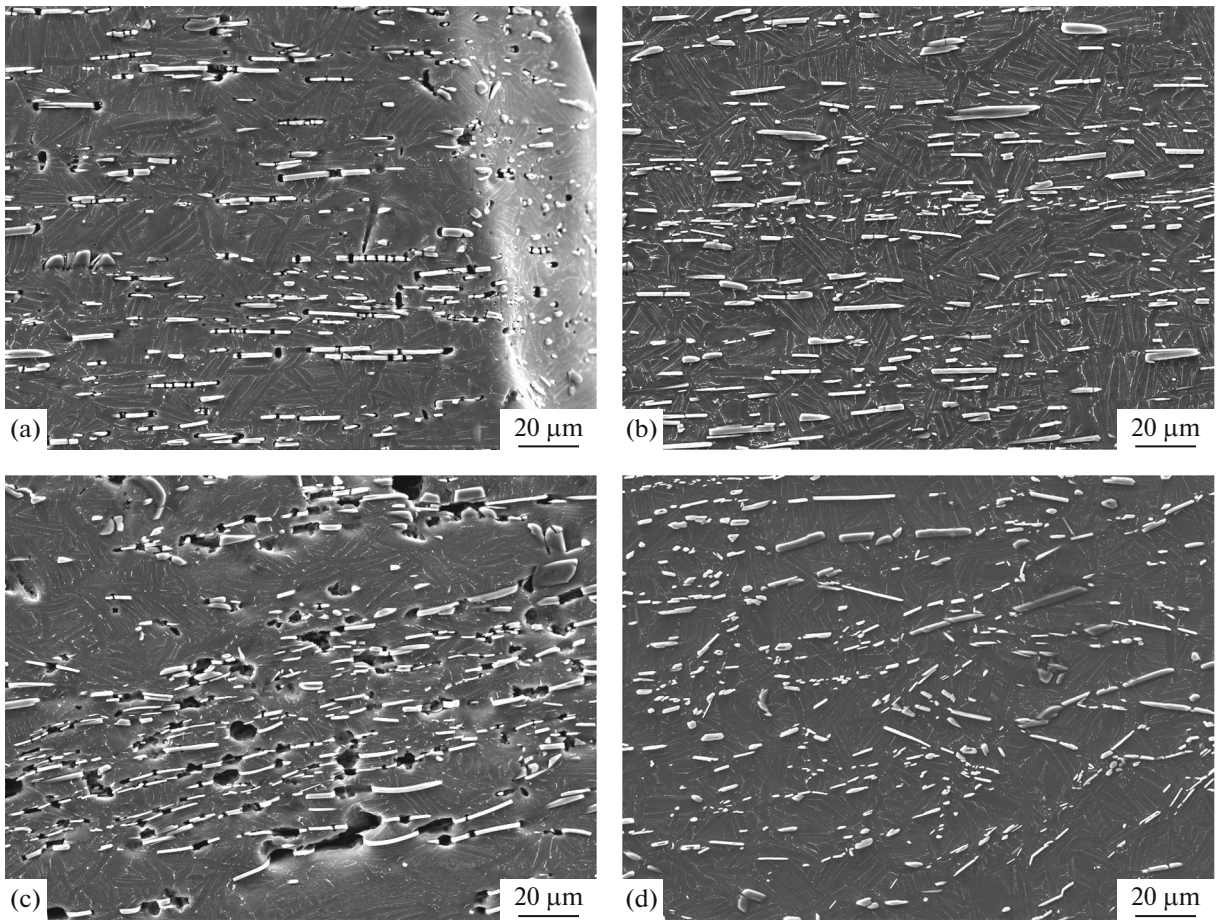


**Fig. 6.** Microstructure of the VT18U/TiB composite subjected to 3D forging and heat treatment after tensile tests at (a, b) $T = 20°C$ ($\delta = 7\%$) and (c, d) $T = 700°C$ ($\delta = 43\%$); (a, c) near and (b, d) far from the fracture zone; the tensile axis is horizontal.

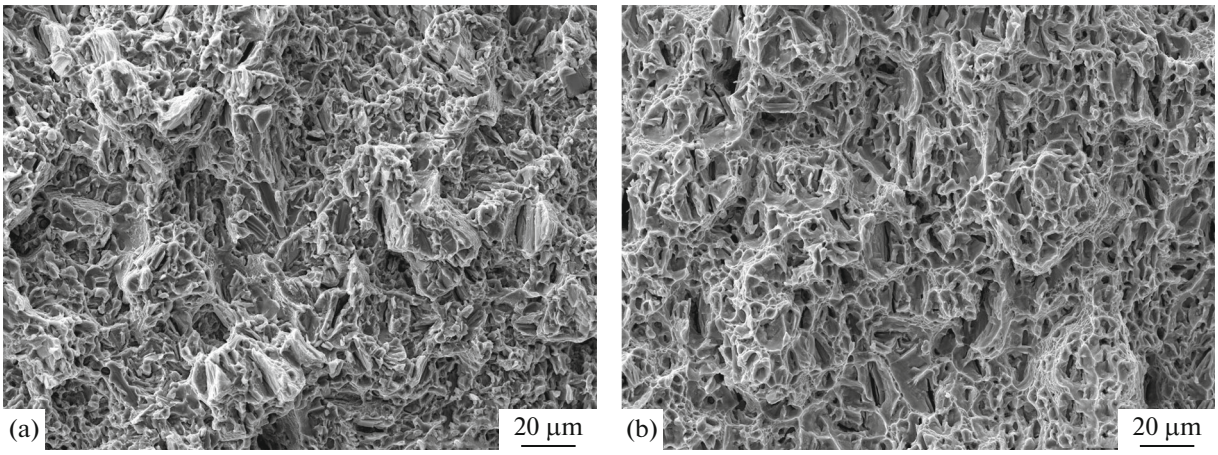


**Fig. 7.** Fracture surface of samples of the VT18U/TiB composite subjected to 3D forging and heat treatment after tensile test at (a) $T = 20°C$ and (b) $T = 600°C$.

distribution of borides after 3D forging (by a decrease in the distance between borides) and by a lower size of the $\alpha + \beta$ colonies after the final heat treatment.

The high adhesion strength of the boundaries between the titanium matrix and TiB fibers is retained with an increase in the test temperature, which is con-

firmed by earlier studies. This is clearly important for creating heat-temperature composite materials based on Ti/TiB, which are able to work at $T \geq 600°C$.

There is great interest in further studies investigating the direction of the selection of the most high-temperature matrix material and an efficient method of deformation of CMs, which would provide the isotropic properties and retain high adhesive strength of the boundaries between the matrix and the reinforcement fibers at elevated temperatures.

## CONCLUSIONS

In this paper, we have studied a new material based on the VT18U/TiB composite prepared by casting and subjected to deformation and heat treatments. The following conclusions can be drawn from our results.

(1) The VT18U/6.5 vol % TiB composite material was subjected to isothermal 2D and 3D forging at temperatures of the $\alpha + \beta$ phase field followed by heat treatment in the $\beta$ and $\alpha + \beta$ fields. We found that the 2D forging leads to the formation of a sharp texture of fibers and the retention of their high aspect ratio. The 3D forging results in a random orientation and strong breaking of borides.

(2) The deformation and heat treatment of the VT18U/6.5 vol % TiB composite provide an appreciable strengthening (by 17.3–32.0%) at $T = 20–700°C$ and a significant increase in the creep resistance at temperatures $T = 550–600°C$ compared to the matrix alloy with the retention of an acceptable plasticity ($\delta = 5.2–7.0\%$) at room temperature.

(3) The strengthening of the composite is caused by the high adhesion strength of boundaries between the matrix and TiB fibers, which is retained at elevated temperatures. During tensile deformation at room and elevated temperatures, the failure mechanism of the VT18U/6.5 vol % TiB composite material was brittle fracture of the TiB fibers followed by the ductile fracture of the matrix material.

## ACKNOWLEDGMENTS

The work was carried out under the state assignment to the Institute for Metals Superplasticity Problems, Russian Academy of Sciences (no. AAAA-A17-117041310215-4) and was partly supported by the Russian Foundation for Basic Research (project no. 16-33-00723 mol_a). The experimental studies were carried out at the Center of Collaborative Access of the Institute for Metals Superplasticity Problems, Russian Academy of Sciences.

## REFERENCES

1. *New Materials*, Ed. by Yu. S. Karabasov (MISIS, Moscow, 2002) [in Russian].
2. T. M. T. Godfrey, P. S. Goodwin, and C. M. Ward-Close, "Titanium particulate metal matrix composites. Reinforcement, production methods and mechanical properties," Adv. Eng. Mater. **2**, 85–92 (2000).
3. K. S. R. Chandran, K. B. Panda, and S. S. Sahay, "$TiB_w$-reinforced Ti composites: processing, Properties, application prospects, and research needs," JOM **56** (5), 42–48 (2004).
4. M. Gorsse and D. B. Miracle, "Mechanical properties of Ti–6Al–4V/TiB composites with randomly oriented and aligned TiB reinforcements," Acta Mater. **51**, 2427–2442 (2003).
5. S. Abkowitz, S. M. Abkowitz, H. Fisher, and P. J. Schwartz, "CermeTi® discontinuously reinforced Ti-matrix composites: Manufacturing, properties, and applications," JOM **56** (5), 37–41 (2004).
6. S. C. Tjong and Y.-W. Mai, "Processing-structure-property aspects of particulate- and whisker-reinforced titanium matrix composites," Comp. Sci. Technol. **68**, 583–601 (2008).
7. X. Guo, L. Wang, M. Wang, J. Qin, D. Zhang, and W. Lu, Effects of degree of deformation on the microstructure, mechanical properties and texture of hybrid-reinforced titanium matrix composites, Acta Mater. **60**, 2656–2667 (2012).
8. C. Zhang, X. Li, S. Zhang, L. Chai, Z. Chen, F. Kong, and Y. Chen, "Effects of direct rolling deformation on the microstructure and tensile properties of the 2.5 vol % ($TiB_w$ + $TiC_p$)/Ti composites," Mater. Sci. Eng., A **684**, 645–651 (2017).
9. J. Qu, C. Zhang, S. Zhang, J. Han, L. Chai, Z. Chen, and Y. Chen, "Relationships among reinforcement volume fraction, microstructure and tensile properties of ($TiB_w$ + $TiC_p$)/Ti composites after ($\alpha + \beta$) forging," Mater. Sci. Eng., A **701**, 16–23 (2017).
10. D. Hill, R. Banerjee, D. Huber, J. Tikey, and H. L. Fraser, "Formation of equiaxed alpha in TiB reinforced Ti alloy composites," Scr. Mater. **52**, 387–392 (2005).
11. C. J. Zhang, F. T. Kong, L. J. Xu, E. T. Zhao, S. L. Xiao, Y. Y. Chen, N. J. Deng, W. Ge, and G. J. Xu, "Temperature dependence of tensile properties and fracture behavior of as rolled TiB/Ti composite sheet," Mater. Sci. Eng., A **556**, 962–969 (2012).
12. I. Sen, L. Maheshwari, S. Tamirisakandala, D. B. Miracle, and U. Ramamurty, "Micromechanisms of damage in a hypereutectic Ti–6Al–4V–B alloy," Mater. Sci. Eng., A **518**, 162–166 (2009).
13. O. M. Ivasishin, R. V. Teliovych, V. G. Ivanchenko, S. Tamirisakandala, and D. B. Miracle, "Processing, microstructure, texture, and tensile properties of the Ti–6Al–4V–1.55B eutectic alloy," Metall. Mater. Trans. A. **39**, 402–416 (2008).
14. V. M. Imayev, R. A. Gaisin, E. R. Gaisina, R. M. Imayev, H.-J. Fecht, and F. Pyczak, "Effect of hot forging on microstructure and tensile properties of Ti–TiB

based composites produced by casting," Mater. Sci. Eng., A **609**, 34–41 (2014).

15. V. M. Imayev, R. A. Gaisin, and R. M. Imayev, "Effect of boron additions and processing on microstructure and mechanical properties of a titanium alloy Ti–6.5Al–3.3Mo–0.3Si," Mater. Sci. Eng., A **641**, 71–83 (2015).
16. H. Attar, S. Ehtemam-Haghighi, D. Kent, I. V. Okulov, H. Wendrock, M. Boenisch, A. S. Volegov, M. Calin, J. Eckert, and M. S. Dargusch, "Nanoindentation and wear properties of Ti and Ti–TiB composite materials produced by selective laser melting," Mater. Sci. Eng., A **688**, 20–26 (2017).
17. M. Ozerov, M. Klimova, A. Kolesnikov, N. Stepanov, and S. Zherebtsov, "Deformation behavior and microstructure evolution of a Ti/TiB metal-matrix composite during high-temperature compression tests," Mater. Des. **112**, 17–26 (2016).
18. C. Zhang, F. Kong, Sh. Xiao, H. Niu, L. Xu, and Y. Chen, "Evolution of microstructural characteristic and tensile properties during preparation of TiB/Ti composite sheet," Mater. Des. **36**, 505–510 (2012).
19. M. J. Koo, J. S. Park, M. K. Park, T. K. Kyung, and S. H. Hong, "Effect of aspect ratios of in situ formed TiB whiskers on the mechanical properties of $TiB_w$/Ti–6Al–4V composites," Scr. Mater. **66**, 487–490 (2012).
20. F. Ma, S. Lu, P. Liu, W. Li, X. Liu, X. Chen, K. Zhang, D. Pan, W. Lu, and D. Zhang, "Microstructure and mechanical properties variation of TiB/Ti matrix composite by thermo-mechanical processing in beta phase field," J. Alloys Compd. **695**, 1515–1522 (2017).
21. H. L. Cox and H. L. Br, "The elasticity and strength of paper and other fibrous materials," Brit. J. Appl. Phys. **3**, 72–79 (1952).
22. R. A. Gaisin, V. M. Imaev, and R. M. Imaev, "Microstructure and mechanical properties of composite VT25U/TiB, obtained by in situ method using casting and hot forging," Pis'ma Mater. **7**, 186–192 (2017).
23. R. A. Gaisin, V. M. Imayev, and R. M. Imayev, "Effect of hot forging on microstructure and mechanical properties of near α titanium alloy/TiB composites produced by casting," J/ Alloys Compd. **723**, 385–394 (2017).
24. V. M. Imayev, R. A. Gaisin, and R. M. Imayev, "Effect of boron addition on formation of a fine-grained microstructure in commercially pure titanium processed by hot compression," Mater. Sci. Eng., A **639**, 691–698 (2015).
25. A. Kelly and W. R. Tyson, "Tensile properties of fibre-reinforced metals: Copper/tungsten and copper/molybdenum," J. Mech. Phys. Solids **13**, 329–350 (1969).
26. H. B. Feng, Y. Zhou, D. C. Jia, Q. C. Meng, and J. C. Rao, "Growth mechanism of in situ TiB whiskers in spark plasma sintered TiB/Ti metal matrix composites," Cryst. Growth Des. **6**, 1626–1630 (2006).

*Translated by O. Golosova*